



NRC Publications Archive Archives des publications du CNRC

Analysis of the aerodynamic performance of a morphing wing-tip demonstrator using a novel nonlinear Vortex Lattice Method

Oliviu, Sugar gabor; Koreanschi, Andreea; Botez, Ruxandra M.; Mamou, Mahmoud; Mebarki, Youssef

This publication could be one of several versions: author's original, accepted manuscript or the publisher's version. / La version de cette publication peut être l'une des suivantes : la version prépublication de l'auteur, la version acceptée du manuscrit ou la version de l'éditeur.

For the publisher's version, please access the DOI link below. / Pour consulter la version de l'éditeur, utilisez le lien DOI ci-dessous.

Publisher's version / Version de l'éditeur:

<https://doi.org/10.2514/6.2016-4036>

34th AIAA Applied Aerodynamics Conference, 2016-06-13

NRC Publications Record / Notice d'Archives des publications de CNRC:

<https://nrc-publications.canada.ca/eng/view/object/?id=95c88c23-d712-409c-9707-643fa13099d4>

<https://publications-cnrc.canada.ca/fra/voir/objet/?id=95c88c23-d712-409c-9707-643fa13099d4>

Access and use of this website and the material on it are subject to the Terms and Conditions set forth at

<https://nrc-publications.canada.ca/eng/copyright>

READ THESE TERMS AND CONDITIONS CAREFULLY BEFORE USING THIS WEBSITE.

L'accès à ce site Web et l'utilisation de son contenu sont assujettis aux conditions présentées dans le site

<https://publications-cnrc.canada.ca/fra/droits>

LISEZ CES CONDITIONS ATTENTIVEMENT AVANT D'UTILISER CE SITE WEB.

Questions? Contact the NRC Publications Archive team at

PublicationsArchive-ArchivesPublications@nrc-cnrc.gc.ca. If you wish to email the authors directly, please see the first page of the publication for their contact information.

Vous avez des questions? Nous pouvons vous aider. Pour communiquer directement avec un auteur, consultez la première page de la revue dans laquelle son article a été publié afin de trouver ses coordonnées. Si vous n'arrivez pas à les repérer, communiquez avec nous à PublicationsArchive-ArchivesPublications@nrc-cnrc.gc.ca.



See discussions, stats, and author profiles for this publication at: <https://www.researchgate.net/publication/303903086>

Analysis of the Aerodynamic Performance of a Morphing Wing-Tip Demonstrator Using a Novel Nonlinear Vortex...

Conference Paper · June 2016

DOI: 10.2514/6.2016-4036

CITATION

1

READS

77

5 authors, including:



Andreea Koreanschi

École de Technologie Supérieure

32 PUBLICATIONS 91 CITATIONS

SEE PROFILE



Ruxandra Mihaela Botez

École de Technologie Supérieure

415 PUBLICATIONS 1,754 CITATIONS

SEE PROFILE



Mahmoud Mamou

National Research Council Canada

169 PUBLICATIONS 1,392 CITATIONS

SEE PROFILE



Youssef Mebarki

National Research Council Canada

81 PUBLICATIONS 553 CITATIONS

SEE PROFILE

Analysis of the Aerodynamic Performance of a Morphing Wing-Tip Demonstrator Using a Novel Nonlinear Vortex Lattice Method

Oliviu Şugar Gabor, Andreea Koreaschi, Ruxandra Mihaela Botez

*LARCASE Laboratory of Research in Active Control, Avionics and Aeroservoelasticity, Ecole de
Technologie Supérieure, Montreal, QC, H3C1K3, Canada*

and

Mahmoud Mamou, Youssef Mebarki

*Aerodynamics Laboratory, NRC Aerospace, National Research Council Canada, Ottawa, ON,
K1A0R6, Canada*

Abstract

This paper presents the novel nonlinear formulation of the Vortex Lattice Method approach for calculating the aerodynamic properties of lifting surfaces. The mathematical model is constructed by using two-dimensional viscous analyses of the wing span-wise sections, according to strip theory, and then coupling the strip viscous forces with the forces generated by the vortex rings distributed on the wing camber surface, calculated with a fully three-dimensional

vortex lifting law. The numerical results obtained with the proposed method are validated with experimental data and show good agreement in predicting both the lift and pitching moment, as well as in predicting the wing drag. The technology demonstrator was modeled after an aircraft wing tip section, and was fitted with a composite material upper skin whose shape can be morphed, as a function of the flight condition, by four electrical actuators placed inside the wing structure. The nonlinear VLM results were compared with balance forces/moments measurements taken during subsonic wind tunnel tests performed at the National Research Council Canada.

I. Introduction

The reduction of fuel consumption and of greenhouse gasses emissions represents a very important research area for both the aerospace industry and the academia. One possibility for increasing aircraft efficiency and achieving the required reductions is through the new-generation technologies of morphing aircraft. A morphing wing could be deformed according to the flight conditions, thus allowing a multi-point design of the aircraft and achieving optimal lift-to-drag ratios for any conditions encountered during flight.

Researchers have proposed different technological solutions for obtaining the desired wing adaptability, and some concepts achieved important theoretical performance improvements compared to the baseline design. Morphing wings were used to adapt the wing span and airfoil camber [1]-[2], the winglet's cant and toe angles [3], to replace conventional high-lift devices [4]-[5], or even the conventional control surfaces [6]. However, the technology is still in the early stages of development, its technological readiness level is still very low, and only a few

concepts have sufficiently progressed to reach wind tunnel testing, and even fewer have actually been flight tested [7].

The CRIAQ 7.1 project, which took place between 2006 and 2009, was realized following a collaborative effort between teams from the École de Technologie Supérieure (ÉTS), École Polytechnique de Montréal, Bombardier Aerospace, Thales Canada and the National Research Council Canada (CNRC). The objective of the project was to improve and control the laminarity of the flow past a morphing wing in order to obtain a substantial drag reduction [8]. In this project, the active structure of the morphing wing consisted of a flexible upper surface and a Shape Memory Alloy (SMA) actuator group located inside the wing box, which could morph the flexible skin at two actuation points. [9]. A theoretical study of the morphing wing system in low subsonic flow conditions was performed [10], and very promising results were obtained: the morphing system was able to delay the transition location downstream by up to 30% of the chord, and to reduce the airfoil drag by up to 22%.

Wind tunnel tests were performed in the 2 m × 3 m atmospheric closed circuit subsonic wind tunnel at CNRC. The wind tunnel measurements were analyzed to assess the validity of the numerical wing optimizations [11] and the designed control techniques [12]. Two control approaches were used for providing the optimal SMA actuator displacements for each different flight condition. In the open loop configuration, the desired displacements were directly imposed on the system [13], while a novel, adaptive, neuro-fuzzy approach which was used to predict and control the morphing wing performance [14]. In the closed loop configuration, the displacements were automatically determined as a function of the pressure readings from the wing upper surface [15]-[16].

Recently, research on the capabilities of morphing wings equipped with flexible upper surfaces included the optimization of the ATR42 regional aircraft airfoil [17] and of the Hydra Technologies S4 Unmanned Aerial System (UAS) airfoil [18]. Both cases obtained notable transition delays of up to 20% of the chord and significant drag reductions of up to 15%. In order to obtain three-dimensional wing performance improvements with upper surface morphing, a three dimensional, non-linear numerical extension of the classic lifting line theory, coupled with a two-dimensional viscous flow solver was developed [19]. A study of the UAS-S4 wing revealed that for typical cruise and surveillance flight conditions, the morphing wing could provide drag reductions of up to 5% [20].

The Vortex Lattice Method (VLM) represents a numerical method for calculating the aerodynamic characteristics of wings [21]. Together with the Doublet Lattice Method (DLM), they represent computational approaches of the lifting surface theory, in which the wing is modeled by a zero-thickness solid surface and a free wake, in these regions the singularity solutions of Laplace's equation for the fluid velocity potential being distributed. In recent years, researchers proposed methods for increasing the VLM accuracy by introducing viscous flow correction terms.

In [22], a method for using correction factors to improve the accuracy of the vortex lattice method is presented. The positions of the control points of each surface panel were displaced based on steady-state pressure distributions obtained from high-fidelity CFD computations or from wind tunnel tests data. Ref. [23] presents a wing optimization procedure based on a surrogate model constructed from a corrected low-fidelity aerodynamic model. The aerodynamic model was constructed using a VLM coupled one-way with a two-dimensional compressible viscous analysis of the wing airfoil, while the surrogate model was created using response-

surface methodologies. A quasi-three dimensional aerodynamic solver which provided accurate wing drag results with low computational costs was developed in [24]-[25]. The method used a vortex lattice method coupled one-way with two-dimensional strip analyses. Validation tests proved that the results obtained were in good agreement with high-fidelity CFD results. The method was then used for the multidisciplinary design optimization of the wing shape of a regional passenger aircraft.

II. The nonlinear Vortex Lattice Method

A. The mathematical model

Within the framework of the VLM approach [21], the singularity element is the vortex line solution of the incompressible potential flow equation, while the imposed boundary condition is that of zero flow in the direction normal to the wing's solid surface. The unknown intensities of all vortex rings (or horseshoe vortices) distributed over the wing surface are determined by requiring that the boundary condition be satisfied for the collocation points of the two-dimensional lattice of surface panels:

$$\left(\mathbf{V}_\infty + \sum_{j=1}^N \Gamma_j \mathbf{v}_{ij} \right) \cdot \mathbf{n}_i = 0 \quad i = 1, 2, \dots, N \quad (1)$$

In Equation (1), \mathbf{V}_∞ is the freestream velocity, N is the total number of vortex rings distributed over the wing surface, \mathbf{v}_{ij} is the velocity induced by the unit strength vortex ring j at the i^{th} panel collocation point and \mathbf{n}_i is the surface normal vector calculated at the i^{th} panel collocation point.

In the new nonlinear VLM approach, the intensities of the vortex rings obtained by solving the linear system presented in Equation (1) are adjusted using nonlinear viscous data. For each vortex ring, a correction $\Delta\Gamma$ is defined, so that the final values of the vortex intensities become:

$$\Gamma_j \rightarrow \Gamma_j + \Delta\Gamma_j \quad j = 1, 2, \dots, N \quad (2)$$

The corrected vortex rings' intensities cannot satisfy the same boundary conditions as the uncorrected intensities, since Equation (1) leads to a uniquely determined solution. By considering that a variation in the intensity of a vortex ring determines a variation in the velocities induced by that vortex ring, the introduction of the $\Delta\Gamma_j$ corrections is followed by the introduction of a secondary induced velocity field over the wing surface. Thus, for the nonlinear VLM approach, Equation (1) becomes:

$$\left(\mathbf{v}_\infty + \sum_{j=1}^N (\Gamma_j + \Delta\Gamma_j) \mathbf{v}_{ij} + \mathbf{V}_i^T \right) \cdot \mathbf{n}_i = 0 \quad (3)$$

In Equation (3), the unknown added velocity $\mathbf{V}_i^T = V_i^T \mathbf{n}_i$ determined by the introduction of the vortex rings' intensity corrections can be considered as a type of surface transpiration velocity, being a direct measure of the alteration of the classic VLM boundary condition.

In order to obtain the second set of equations needed for the problem resolution, a nonlinear viscous pressure coefficient distribution is required. This data is obtained by performing a two-dimensional strip analysis of the wing. For each strip, a control point is defined, placed at the middle of the three-quarter chord line of the strip and projected on the camber line of the local strip airfoil. The span-wise strips are analysed under the local flow conditions (Reynolds

number, effective angle of attack), using a two-dimensional viscous flow solver. The local flow conditions are calculated at the strip's previously defined control point.

$$CP_i^{visc} = f(airfoil_i, Re_i, \|\mathbf{V}_i\|, \alpha_i), \quad i = 1, 2, \dots, N_Y \quad (4)$$

The strip's local effective angle of attack is calculated using Equation (5), where \mathbf{cs}_i is the unit vector in the direction of the chord, and \mathbf{ns}_i is the unit vector in the direction normal to the chord, both vectors being in the plane of the local airfoil of the i^{th} strip.

$$\alpha_i = \tan^{-1} \left(\frac{\mathbf{V}_i \cdot \mathbf{ns}_i}{\mathbf{V}_i \cdot \mathbf{cs}_i} \right) = \tan^{-1} \left[\frac{(\mathbf{V}_\infty + \sum_{j=1}^N (\Gamma_j + \Delta\Gamma_j) \mathbf{v}_{ij}) \cdot \mathbf{ns}_i}{(\mathbf{V}_\infty + \sum_{j=1}^N (\Gamma_j + \Delta\Gamma_j) \mathbf{v}_{ij}) \cdot \mathbf{cs}_i} \right] \quad (5)$$

From the pressure coefficient distribution over the local strip airfoil, the pressure coefficient difference between the lower and upper surfaces can be determined for the collocation points of the wing panels that are placed on each specific wing strip.

The equations needed to calculate the vortex rings' intensity corrections are constructed from the assumption that for all N panels on the wing surface, the pressure coefficient variation obtained from the vortex rings' intensities is equal to the nonlinear viscous pressure coefficient variation obtained from the wing strip analysis. For all panels, the following equality is written:

$$\Delta CP_i = \Delta CP_i^{visc} \quad i = 1, 2, \dots, N \quad (6)$$

The pressure coefficient variation for any panel on the wing surface can be written as function of the aerodynamic force generated by that panel:

$$\Delta CP_i = - \frac{\mathbf{F}_i \cdot \mathbf{n}_i}{A_i Q_\infty} \quad (7)$$

In Equation (7), \mathbf{F}_i is the aerodynamic force generated by all the vortex lines placed on the panel, \mathbf{n}_i is the surface normal vector calculated at the panel collocation point, A_i is the panel area and Q_∞ is the freestream dynamic pressure. By combining Equations (6) and (7):

$$-\mathbf{F}_i \cdot \mathbf{n}_i + A_i Q_\infty \Delta C P_i^{visc} = 0 \quad i = 1, 2, \dots, N \quad (8)$$

The force can be calculated (using the three-dimensional vortex lifting law [26]) as function of the vortex intensity of the current panel and its neighbours (Upstream, Left, Right, Upstream-Left and Upstream-Right), as presented in Equation (9). For certain panels, such as those situated at the wing leading edge or at the wing tips, one or several of the neighbouring panels do not exist, and thus must not included in the calculation of the force.

$$\begin{aligned} \mathbf{F}_i = & \rho(\Gamma_i - \Gamma_U)\mathbf{V}_i \times \boldsymbol{\gamma}_{12} + \rho(\Gamma_i - \Gamma_R)\mathbf{V}_i \times \boldsymbol{\gamma}_{23} + \\ & + \rho(\Gamma_i - \Gamma_L)\mathbf{V}_i \times \boldsymbol{\gamma}_{61} + \rho(\Gamma_U - \Gamma_{UR})\mathbf{V}_i \times \boldsymbol{\gamma}_{34} + \rho(\Gamma_U - \Gamma_{UL})\mathbf{V}_i \times \boldsymbol{\gamma}_{56} \end{aligned} \quad (9)$$

where ρ is the air density, Γ is the intensity of a vortex ring, \mathbf{V}_i is the local velocity at the panel collocation point and $\boldsymbol{\gamma}$ is the supporting geometric segment of a vortex line.

The force given in Equation (9) is then projected onto the direction of the local normal vector, and the resulting expression is rearranged using the scalar triple product and the linear properties of the dot product operator. By introducing the value of the local velocity at the panel collocation point, given by Equation (3), the following expression is obtained for the normal force acting on each of the wing surface panels:

$$\begin{aligned}
\mathbf{F}_i \cdot \mathbf{n}_i &= \rho \left[\mathbf{n}_i \times \left(\mathbf{v}_\infty + \sum_{j=1}^N (\Gamma_j + \Delta\Gamma_j) \mathbf{v}_{ij} \right) \right] \cdot \\
&\cdot [(\Gamma_i - \Gamma_U) \boldsymbol{\gamma}_{12} + (\Gamma_i - \Gamma_R) \boldsymbol{\gamma}_{23} + (\Gamma_i - \Gamma_L) \boldsymbol{\gamma}_{61} + (\Gamma_U - \Gamma_{UR}) \boldsymbol{\gamma}_{34} \\
&+ (\Gamma_U - \Gamma_{UL}) \boldsymbol{\gamma}_{56} + (\Delta\Gamma_i - \Delta\Gamma_U) \boldsymbol{\gamma}_{12} + (\Delta\Gamma_i - \Delta\Gamma_R) \boldsymbol{\gamma}_{23} + (\Delta\Gamma_i - \Delta\Gamma_L) \boldsymbol{\gamma}_{61} \\
&+ (\Delta\Gamma_U - \Delta\Gamma_{UR}) \boldsymbol{\gamma}_{34} + (\Delta\Gamma_U - \Delta\Gamma_{UL}) \boldsymbol{\gamma}_{56}] \quad i = 1, 2, \dots, N
\end{aligned} \tag{10}$$

By introducing the normal force \mathbf{F}_i given by Equation (10) into the equality presented in Equation (8), and coupling the resulting equations with Equations (3) and (1), a nonlinear system of $2N$ equations is obtained:

$$\mathbf{R} = \left\{ \begin{array}{c} \vdots \\ -\mathbf{F}_i \cdot \mathbf{n}_i + A_i Q_\infty \Delta C P_i^{visc} \\ \vdots \\ \vdots \\ \sum_{j=1}^N \mathbf{v}_{ij} \cdot \mathbf{n}_i \Delta\Gamma_j + V_i^T \\ \vdots \end{array} \right\} = \mathbf{0} \tag{11}$$

The unknown variables of the system are the N values of the vortex rings' intensity corrections and the N values of the surface transpiration velocities:

$$\mathbf{X} = \{\dots \Delta\Gamma_i \dots \dots V_i^T \dots\}^T \tag{12}$$

B. The numerical solution procedure

The nonlinear system of equations can be solved using Newton's method [27]. Starting with an initial guess of the solution vector \mathbf{X}^0 , the quality of this estimate can be improved using the following iterative procedure:

$$\mathbf{J}(\mathbf{X}^k)\Delta\mathbf{X} = -\mathbf{R}(\mathbf{X}^k) \quad (13)$$

$$\mathbf{X}^{k+1} = \mathbf{X}^k + \Omega\Delta\mathbf{X}$$

In Equation (13), $\mathbf{J}(\mathbf{X}^k)$ is the Jacobian matrix of first-order partial derivatives, calculated with the current estimate of the solution vector, $-\mathbf{R}(\mathbf{X}^k)$ is the system residual, calculated with the current estimate of the solution vector, $\Delta\mathbf{X}$ is the solution increment and Ω is an under-relaxation factor. The iterative solution procedure continues until the magnitude of the largest residual becomes smaller than the desired convergence criteria.

Starting from the expression of the nonlinear system in Equation (11), the Jacobian matrix can be determined analytically, through laborious but straightforward partial derivatives computations.

The Jacobian matrix is presented in Equation (12), divided in four $N \times N$ partitions:

$$\mathbf{J} = \frac{\partial R_i}{\partial X_k} = \left[\begin{array}{c|c} \frac{\partial(-\mathbf{F}_i \cdot \mathbf{n}_i + A_i Q_\infty \Delta C P_i^{visc})}{\partial \Delta \Gamma_k} & \frac{\partial(-\mathbf{F}_i \cdot \mathbf{n}_i + A_i Q_\infty \Delta C P_i^{visc})}{\partial V_k^T} \\ \hline \frac{\partial(\sum_{j=1}^N \mathbf{v}_{ij} \cdot \mathbf{n}_i \Delta \Gamma_j + V_i^T)}{\partial \Delta \Gamma_k} & \frac{\partial(\sum_{j=1}^N \mathbf{v}_{ij} \cdot \mathbf{n}_i \Delta \Gamma_j + V_i^T)}{\partial V_k^T} \end{array} \right] = \quad (14)$$

$$= \left[\begin{array}{c|c} \frac{\partial(-\mathbf{F}_i \cdot \mathbf{n}_i)}{\partial \Delta \Gamma_k} + A_i Q_\infty \frac{\partial(\Delta C P_i^{visc})}{\partial \Delta \Gamma_k} & \mathbf{0} \\ \hline \mathbf{v}_{ik} \cdot \mathbf{n}_i & \mathbf{I} \end{array} \right]$$

The viscous pressure coefficient difference values were obtained following a two-dimensional strip analysis of the wing, where each strip airfoil was calculated at the corresponding local flow conditions. Assuming incompressible flow, the strip pressure coefficient distribution depends only on the local angle of attack given by Equation (5). It must be observed that the local value of the pressure coefficient difference between the lower and upper surfaces also depends on the

chord-wise position where it is calculated. Thus, the derivative of the pressure coefficient difference can be written as:

$$\left(\frac{\partial \Delta CP^{visc}}{\partial \Delta \Gamma_k}\right)_{for\ panel\ (i)} = \left(\frac{\partial \Delta CP^{visc}}{\partial \alpha_l}\right)_{for\ strip\ (l)\ and\ \left(\frac{X}{C}\right)_{chordwise\ position}} \frac{\partial \alpha_l}{\partial \Delta \Gamma_k} \quad (15)$$

The first right hand side term of Equation (15) can be estimated for each wing strip while performing the two-dimensional strip analysis, and then the values can be interpolated for the current panel i , as a function of the strip l on which the panel is placed and the relative chord-wise position of the panel collocation point on the local airfoil chord. The derivative of the strip angle of attack can be determined based on Equation (5) and is equal to:

$$\frac{\partial \alpha_l}{\partial \Delta \Gamma_k} = \frac{(\mathbf{v}_{lk} \cdot \mathbf{ns}_l)V_c - (\mathbf{v}_{lk} \cdot \mathbf{cs}_l)V_n}{V_c^2 + V_n^2} \quad (16)$$

$$V_n = \left(\mathbf{v}_\infty + \sum_{j=1}^N (\Gamma_j + \Delta \Gamma_j) \mathbf{v}_{lj} \right) \cdot \mathbf{ns}_l \quad (17)$$

$$V_c = \left(\mathbf{v}_\infty + \sum_{j=1}^N (\Gamma_j + \Delta \Gamma_j) \mathbf{v}_{lj} \right) \cdot \mathbf{cs}_l \quad (18)$$

After the determination of the values of the vortex rings' corrections with the iterative Newton procedure described in Equation (13), the aerodynamic force for each panel on the wing surface can be computed with Equation (9), and the total aerodynamic force generated by the lifting surface can be determined by summing the individual panel forces. The total aerodynamic moment generated about a desired reference point can also be computed by summing the individual moments generated about that chosen point by each panel on the wing surface.

Following the wing strip analysis performed as part of the nonlinear solution procedure, the total wing profile drag (also known as parasite drag) can be calculated based on the two-dimensional airfoil drag of each individual strip, by direct numerical integration along the lifting surface spanwise direction.

C. Method convergence study

To verify the influence of the wing surface grid resolution on the converged values of the aerodynamic coefficients, a study was performed using four test wing geometries. The wings were generated using the NACA0012 airfoil and cover four different scenarios: low aspect ratio – low sweep angle, low aspect ratio – high sweep angle, high aspect ratio – low sweep angle and high aspect ratio – high sweep angle. Details on the geometries of the four test wings are presented in Table 1.

Table 1 Details of test wings used for grid convergence study

Detail	Wing 1	Wing 2	Wing 3	Wing 4
Aspect Ratio	4	4	12	10
Sweep Angle	0 deg.	60 deg.	0 deg.	45 deg.
Span	1.00	1.00	4.50	3.20
MAC	0.26	0.26	0.42	0.42
Taper Ratio	0.60	0.60	0.285	0.45

All four tests were performed using the same Newton iteration convergence criterion of 10^{-3} imposed for the maximum residual value. Eight different surface grids of increasing mesh density were generated for each of the geometries, each grid having a constant spacing in both chord-wise and span-wise directions. The total number of cells for the wing semi-span generated

for each of the eight grids, as well as the chord-wise number N_X and span-wise number N_Y are presented in Table 2.

Table 2 Number of cells included in each grid level used for convergence study

Cells	N_X	N_Y	Total
Grid 1	2	4	8
Grid 2	4	8	32
Grid 3	8	16	128
Grid 4	10	20	200
Grid 5	12	15	300
Grid 6	15	30	450
Grid 7	18	35	630
Grid 8	20	40	800

In Figure 1, the variations of the lift coefficient, drag coefficient and pitching moment coefficient about the quarter chord point of the root chord are presented, for the four test wings, as a function of the grid refinement level. For a better visualisation, and in order to provide direct information on the aerodynamic coefficients' variation with the refinement level, all the coefficient values have been normalized using the value obtained for the finest grid, which is Grid 8. The nonlinear VLM approach requires a sufficiently refined grid to achieve results that are grid-independent, as only for the level seven grid refinement are the results for all three aerodynamic coefficients values and for all four wing geometries within 1% of the values obtained with the most refined grid.

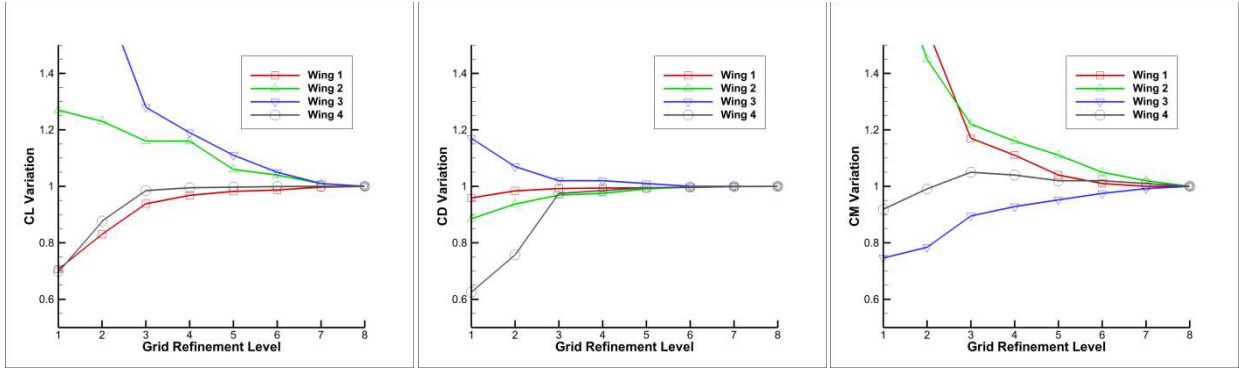


Figure 1 Convergence of the aerodynamic coefficients with grid refinement level

Figure 2 presents the convergence curves for different mesh refinement levels that were presented in Table 2. The first two grid levels did not achieve the desired convergence error of 10^{-3} , and thus only Grid 2 was presented, because it obtained better results. For Grids 7 and 8, the convergence curves are almost superposed, and only Grid 7 was chosen for display, to provide better visualisation. The nonlinear algorithm reaches convergence in five or six iterations, and the minimum residual value varies with the refinement level, achieving lower values on the finer meshes.

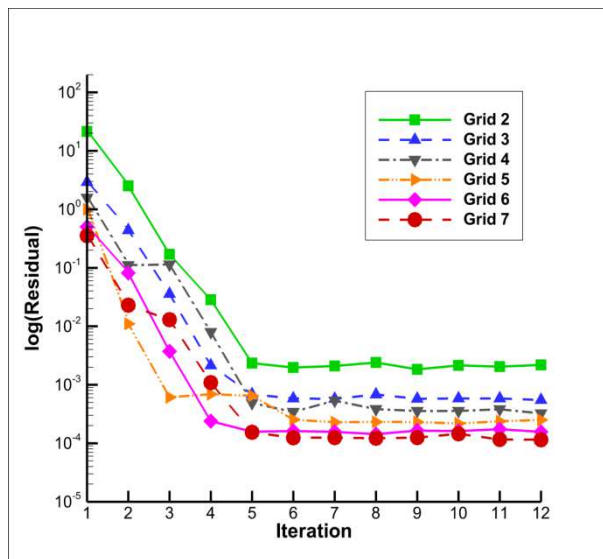


Figure 2 Residual convergence curves with grid refinement level

The nonlinear Vortex Lattice Method described above could be used in the early design phases of subsonic aircraft lifting surfaces, as it provides sufficiently accurate estimations of viscous aerodynamic characteristics for only a fraction of the computational requirements needed to perform a three-dimensional CFD calculation. On a typical desktop workstation, the execution time of the code is only around 1% of the equivalent CFD solution time. When the strip airfoil analyses are performed during execution, then a much greater amount of time is devoted to that task than the amount of time needed to calculate the Jacobian matrix and solve the linear system. Thus, the calculation times can be significantly further reduced by performing the strip calculations in parallel mode, or by using airfoil experimental performance databases instead of running the two-dimensional solver.

III. Validation using wind tunnel experimental results

A. The first validation case

The first viscous flow validation test performed using the nonlinear VLM was done using geometrical and experimental data taken from the NACA Technical Note 1270 [28]. The wing geometry chosen is a high aspect ratio shape with no sweep and a relatively high taper ratio. This wing is constructed using airfoils from the NACA 44-series, with the root section airfoil being a NACA 4422 and the tip section airfoil a NACA 4412. Table 3 presents details about the geometry of the test wing model.

Table 3 Geometric characteristics of the NACA TN 1270 test wing

Aspect Ratio	12
Span	4.56 m
Root Chord	0.5915 m
Taper Ratio	0.285
Sweep angle	0 deg.
Area	1.733 m ²
Tip Twist	-3 deg.
MAC	0.421 m

The experimental results were obtained in the NACA variable density subsonic wind tunnel, for an airspeed of 65 m/s and a Reynolds number equal to 4×10^6 , as calculated with the mean aerodynamic chord value. For the numerical calculations, a mesh of 18 chordwise panels and 35 spanwise panels per wing semi-span was used. The solution of the nonlinear system was obtained with a convergence criterion of 10^{-3} imposed for the maximum residual value.

In Figure 3, the results for the wing lift coefficient, drag coefficient and quarter chord pitching moment coefficient are compared with the experimental data. The calculations were performed with both the classic non-viscous VLM and the new proposed nonlinear coupled VLM algorithm.

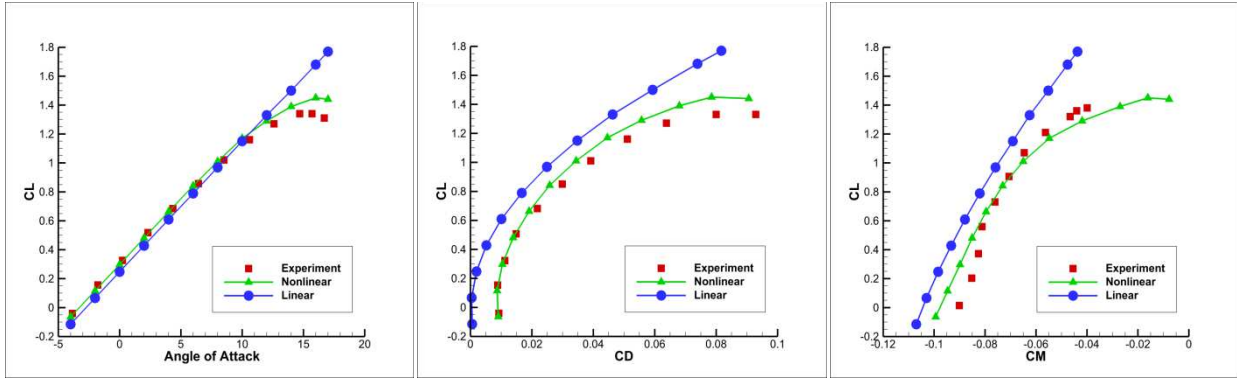


Figure 3 Numerical versus experimental aerodynamic coefficients variation for the NACA TN 1270 wing

The nonlinear VLM code produces an accurate estimation of the viscous lift coefficient slope, and it slightly overestimates the stall angle (16 degrees in the numerical results, versus 14.8 degrees in the experiment) and the maximum lift coefficient value (1.425 in the numerical results, versus 1.340 in the experiment). For the linear VLM, a good estimation of the lift curve slope is obtained, but no stall effects can be computed. The drag coefficient estimation is very accurate for the lift coefficient range below 0.6, after which the numerical code tends to underestimate the drag coefficient values, but it still captures the steep increase associated with stall progression over the wing surface. This accuracy cannot be obtained with the classic VLM which computes only the induced drag because of the lack of viscous effects. Concerning the pitching moment coefficient, the numerical nonlinear VLM results are in closer agreement with the experimental ones, both capturing the linear variation and predicting the nonlinear behaviour characteristic of the higher angles of attack cases. An underestimation of the pitching moment value can be observed for the higher lift coefficient conditions, but the quality of the results is good.

B. The second validation case

The second validation test performed using the nonlinear VLM was done using geometrical and experimental data taken from the NACA Technical Note 1208 [29]. The wing geometry features a high aspect ratio and a high sweep back angle. The model is constructed using a NACA 6-series airfoil section constant along the wingspan. The geometrical characteristics of the test wing are presented in Table 4.

Table 4 Geometric characteristics of the NACA TN 1208 test wing

Aspect Ratio	8
Span	3.23 m
Root Chord	0.5573 m
Taper Ratio	0.45
Sweep angle	45 deg.
Area	1.305 m ²
Tip Twist	0 deg.
MAC	0.421 m

As for the previous validation case, the experimental results were obtained in the NACA variable density subsonic wind tunnel, for an airspeed of 65 m/s and a Reynolds number of 4×10^6 . The numerical results were obtained using a mesh of 18 chordwise panels and 35 spanwise panels per wing semi-span and the convergence criterion of 10^{-3} imposed for the maximum residual value.

In Figure 4, the results for the wing lift coefficient and quarter chord pitching moment coefficient are compared with the experimental data. Drag coefficient data was not provided in the reference to allow for a comparison.

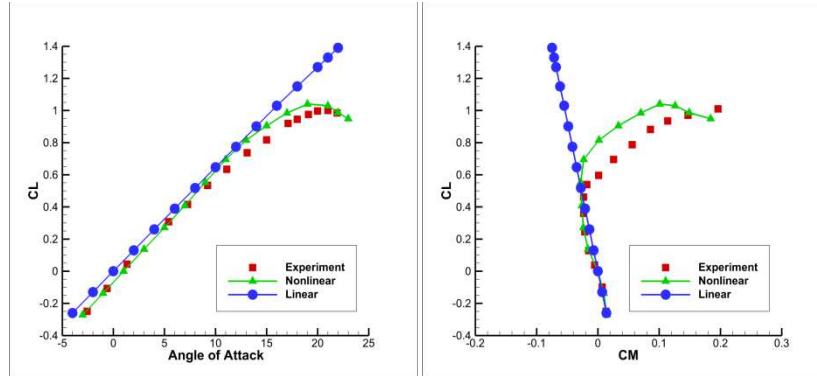


Figure 4 Numerical versus experimental aerodynamic coefficients variation for the NACA TN 1208 wing

The viscous lift coefficient slope predicted by the nonlinear VLM is slightly higher than the experimental value, with a lift overestimation for angles of attack higher than 10 degrees. There is an underestimation of the stall angle (21 degrees for the experiment, versus 19.5 degrees in the numerical results), but a very good agreement exists for the maximum lift coefficient (1.01 for the experiment, versus 1.04 in the numerical results). Improvements can be observed over the classic VLM, both in the ability of predicting nonlinear lift variations close to stall, but also in general agreement of the lift curve. The linear variation of the pitching moment coefficient is very well captured, but there are some differences for the nonlinear higher lift conditions, where the swept back wing experiences an early tip stall phenomenon. As this behaviour is difficult to accurately capture, it is responsible for the numerical over-prediction of both pitching moment and lift coefficients. However, there is an important quality improvement over the linear VLM, especially concerning the high angle of attack characteristics of the high-sweep wing.

C. The third validation case

The third viscous flow validation test performed using the nonlinear VLM was done using geometrical and experimental data taken from the NACA Research Memorandum L50F16 [30].

The wing geometry chosen is a very low aspect ratio shape with high sweep angle. This wing is constructed using the NACA 65A006 airfoil. Table 5 presents details about the geometry of the test wing model.

Table 5 Geometric characteristics of the NACA RM L50F16 test wing

Aspect Ratio	2
Span	0.65 m
Root Chord	0.4066 m
Taper Ratio	0.60
Sweep angle	45 deg.
Area	0.211 m ²
Tip Twist	0 deg.
MAC	0.332 m

The experimental results were obtained in the NACA variable density subsonic wind tunnel, for an airspeed of 35 m/s and a Reynolds number equal to 6×10^6 , as calculated with the mean aerodynamic chord value. For the numerical calculations, a mesh of 18 chordwise panels and 35 spanwise panels per wing semi-span was used. The solution of the nonlinear system was obtained with a convergence criterion of 10^{-2} imposed for the maximum residual value.

In Figure 5, the results for the wing lift coefficient, drag coefficient and quarter chord pitching moment coefficient are compared with the experimental data. The calculations were performed with both the classic non-viscous VLM and the new proposed nonlinear coupled VLM algorithm.

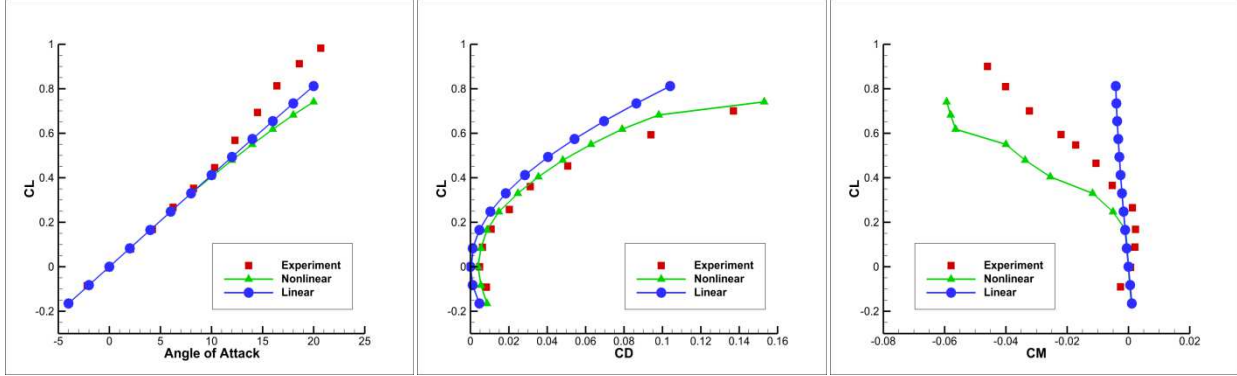


Figure 5 Numerical versus experimental aerodynamic coefficients variation for the NACA RM L50F16 wing

A very good prediction of the lift coefficient exists for angles of attack smaller than 10 degrees. When the angle of attack increases above this value, the lift values predicted by the nonlinear code are smaller than the experimental ones. The classic VLM obtained a slightly better estimation of the lift coefficient for angles of attack higher than 10 degrees, but an under-prediction still exists. Concerning the drag coefficient estimation, there is a very good match between the nonlinear VLM results and the experimental data, especially for lift coefficient values smaller than 0.4, but the overall quality of the numerical results remains for the entire analysis range. The improvement obtained by considering the wing profile drag coefficient is visible from the comparison with the linear VLM drag prediction. The pitching moment coefficient results obtained by the non-linear VLM code are good for the test cases having a lift coefficient smaller than 0.3. For the rest of the analysis range, the non-linear moment variation is captured by the numerical results, but the predicted values are much smaller than the experimental measurements. The classic VLM results are also good for C_L smaller than 0.3, but the moment variation remains linear for the entire range, as expected.

IV. Results for the CRIAQ MDO 505 morphing wing

A. Description of the CRIAQ MDO 505 project

The CRIAQ MDO 505 project is performed as a continuation of the CRIAQ 7.1 project on adaptive upper-surface wing concept. In this project a real wing structure was considered and designed following structural and materials optimizations based on new aerodynamic optimization constraints and new morphing skin control challenges, using an electrical actuation system along with classical and adaptive ailerons. It is a multiple partners project involving an international collaboration between Canadian and Italian industries, universities and research centres (Bombardier Aerospace, Thales Canada and Alenia Aeronautica, on the industry side, École de Technologie Supérieure, École Polytechnique de Montreal and the University of Naples, on the academic side, and CNRC and the Italian Institute for Aerospace Research CIRA on the research centres side).

The novelty of the CRIAQ MDO 505 project consists in the design, analysis and manufacturing of a wind tunnel model with the structural and aerodynamic properties of a real aircraft wing-tip section. The full-scale morphing wing model is a structure with a 1.5 m span and a 1.5 m root chord, a taper ratio of 0.72 and a leading and trailing edges sweep angle of 8° . The wing box and internal structure (spars, ribs, and lower skin) was manufactured from aluminum alloy material, while the adaptive upper surface was positioned between 20% and 65% of the wing chord. The adaptive upper surface skin was specifically designed and optimised for the project. The adaptive skin was manufactured using carbon fibre composite materials [31]. Figure 6 presents the concept and the structural elements of the morphing wing model.

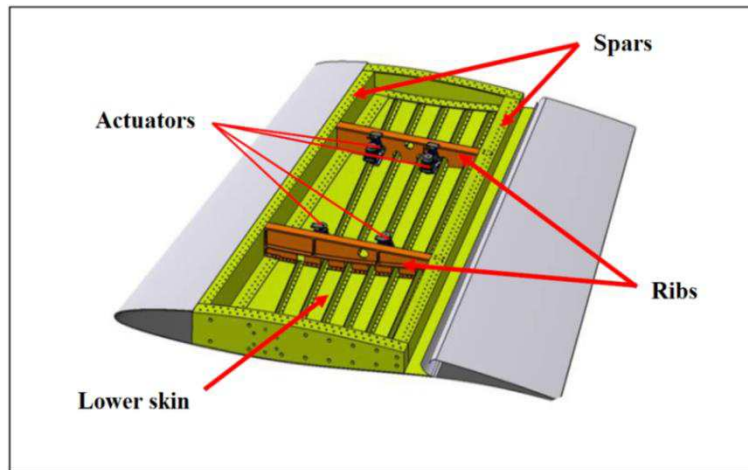


Figure 6 Structural elements of the CRIAQ MDO 505 morphing wing concept (the morphing skin is not shown in the figure)

The deformation of skin shape, driven by actuators placed inside the wing box structure, is a function of the flight condition (defined in terms of Mach number, Reynolds number and angle of attack). These actuators were specifically designed and manufactured to meet the project requirements. Four electric actuators were installed on two actuation lines; two actuators each, placed at 37% and 75% of the wing span, fixed to the ribs and to the composite skin. Each actuator has the ability to operate independently from the others. On each actuation line, the actuators were positioned at 32% and 48% of the local wing chord. The aileron's articulation was located at 72% of the chord, and it was able to undergo a controlled deflection between -7° and $+7^\circ$.

The wind tunnel tests were performed at the 2 m x 3 m atmospheric closed circuit subsonic wind tunnel of the National Research Council Canada. The tunnel allows blowing speeds up to a Mach number of 0.33, at atmospheric pressure. Figure 7 presents the CRIAQ MDO 505 morphing wing model installed in the tunnel test section, viewed from both the leading edge (left figure) and the trailing edge (right figure).



Figure 7 MDO 505 wing model setup in the wind tunnel test section

B. Validation against experimental data for un-deformed wing

The cases that were optimized, analysed and experimentally tested are presented in Table 6. The Reynolds numbers that correspond to the two Mach numbers are 4.28×10^6 and 5.27×10^6 . A downwards aileron deflection was considered positive, while an upwards aileron deflection was considered negative.

In Figures 8 to 10, the results obtained with the nonlinear VLM algorithm for the wing lift coefficient, drag coefficient and the pitching moment coefficient about the one-third of the root chord point are compared with the experimentally measured data. The results are presented for all cases included in Table 6, for the un-deformed wing geometries (the upper skin actuator displacements set to 0).

Table 6 Cases that were analysed and experimentally tested

Mach	Delta [°]	Angle of Attack [°]										
		-	-0.5	0	0.5	1	1.5	2	2.5	3	-	-
0.15	0	-	-0.5	0	0.5	1	1.5	2	2.5	3	-	-
0.20	4	-1.5	-	0	0.5	1	1.5	2	2.5	-	-	-
0.20	-4	-	-	0	0.5	1	1.5	2	2.5	3	4	5

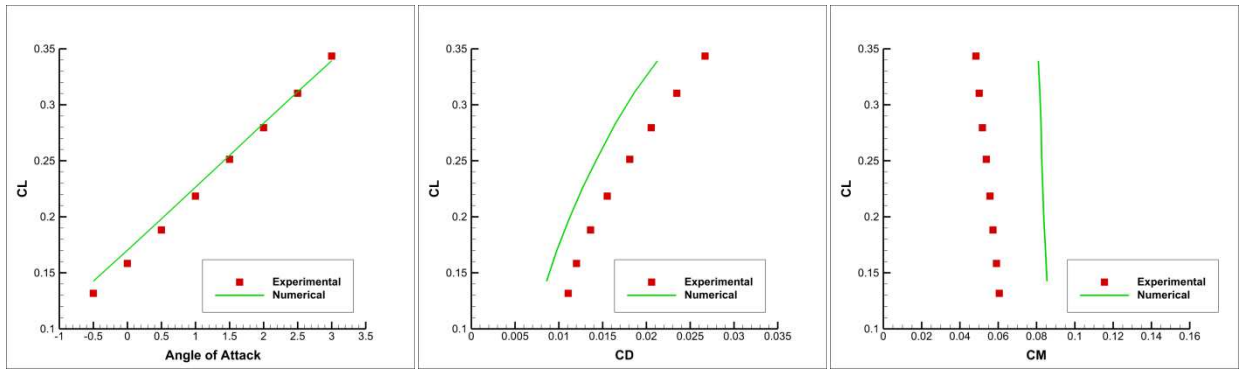


Figure 8 Numerical versus experimental aerodynamic coefficients variation for the wing with no aileron deflection

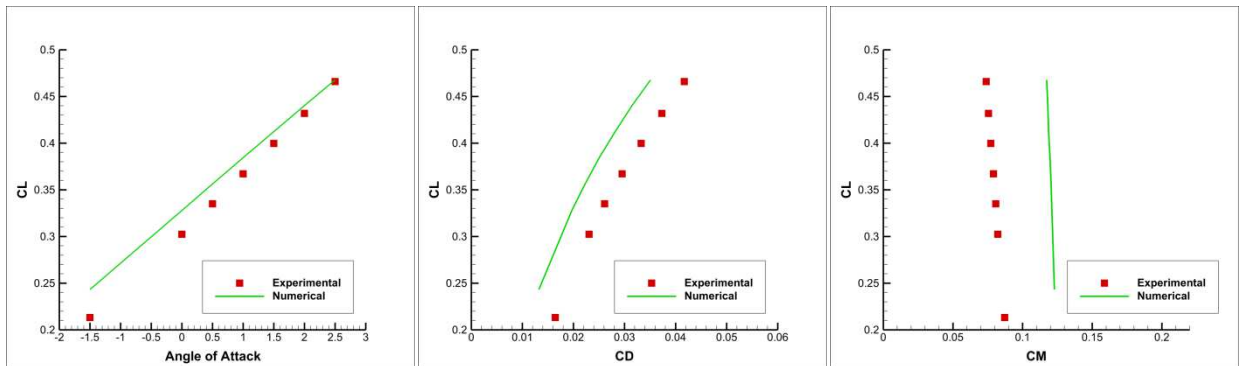


Figure 9 Numerical versus experimental aerodynamic coefficients variation for the wing with aileron deflected 4 degrees downwards

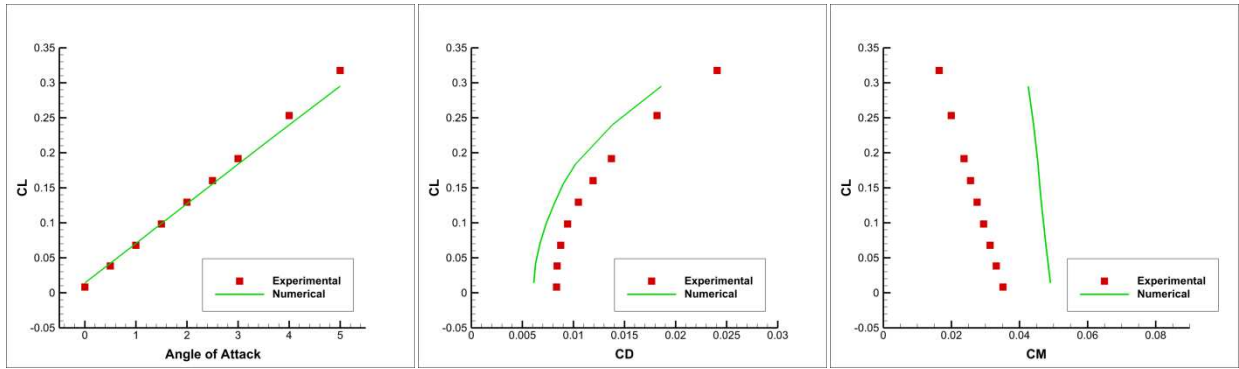


Figure 10 Numerical versus experimental aerodynamic coefficients variation for the wing with aileron deflected 4 degrees upwards

For the cases with no aileron deflection (Figure 8) and with 4 degrees upwards deflection (Figure 10), there is a very good agreement between the numerically predicted lift coefficient and the experimental values. When the aileron is deflected downwards at 4 degrees (Figure 9), there is a difference in the lift curve slope and a numerical overestimation of the lift coefficient for the lower angle of attack values. The cause for this discrepancy is still being analysed. Concerning the drag coefficient, the numerical prediction is always underestimated, but accurately follows the experimental variation as function of the lift coefficient, for all three aileron deflection angles. A possible explanation for this difference is the observed tendency of the two-dimensional viscous flow solver (used for performing the strip analyses) to overestimate the extent of laminar flow over the airfoil surface with comparison to experimental measurements, and thus produce smaller profile drag values. The pitching moment coefficient about the one-third of the root chord point prediction is overestimated by the numerical method. For the cases with no aileron deflection and with 4 degrees downwards deflection (Figures 8 and 9), the slope of moment variation with the lift coefficient is also accurately determined.

C. The morphing wing results

The core concept of an active morphing of the wing upper surface is to provide an optimized airfoil shape for each flight condition. A single point optimization must be performed for each combination of Mach number, Reynolds number and angle of attack. This procedure increases the aerodynamic performance of the shape-changing airfoil (with respect to the desired optimization objective) compared to the multi-point designed baseline airfoil. Aerodynamic optimizations were performed to determine the displacements driven by the electrical actuators required to improve the performance of the morphing wing with respect to the original wing. In order to greatly reduce calculation times, the aerodynamic optimizations were performed under two-dimensional flow assumption using the XFOIL solver [32] and an in-house genetic algorithm optimizer [33], for local flow conditions (local Reynolds number and angle of attack) corresponding to the mean aerodynamic chord of the wing model [34]. For the numerical optimizations, the upper skin shapes were approximated using cubic splines, as function of the actuator displacements. Due to constraints related to structural rigidity of the composite skin, the actuator displacements were limited to ± 3.5 mm, while the maximum difference between the two displacements was limited to 6 mm. The two-dimensional optimizations that determined the electrical actuators displacements were performed with the objective of controlling the extent of laminar flow on the upper surface of the wing model and thus improving the drag characteristics of the morphing wing.

In Figures 11 to 13, a comparison is presented between the original and morphed wing geometries, for the total drag coefficient (left picture) and the profile drag coefficient at the 40% of the span section (right picture). The results presented include both the numerically calculated drag coefficients and the experimentally measured data. The results are presented for all cases

included in Table 6, and the lift and pitching moment coefficients are not included because of the negligible effect of the upper surface morphing on their values.

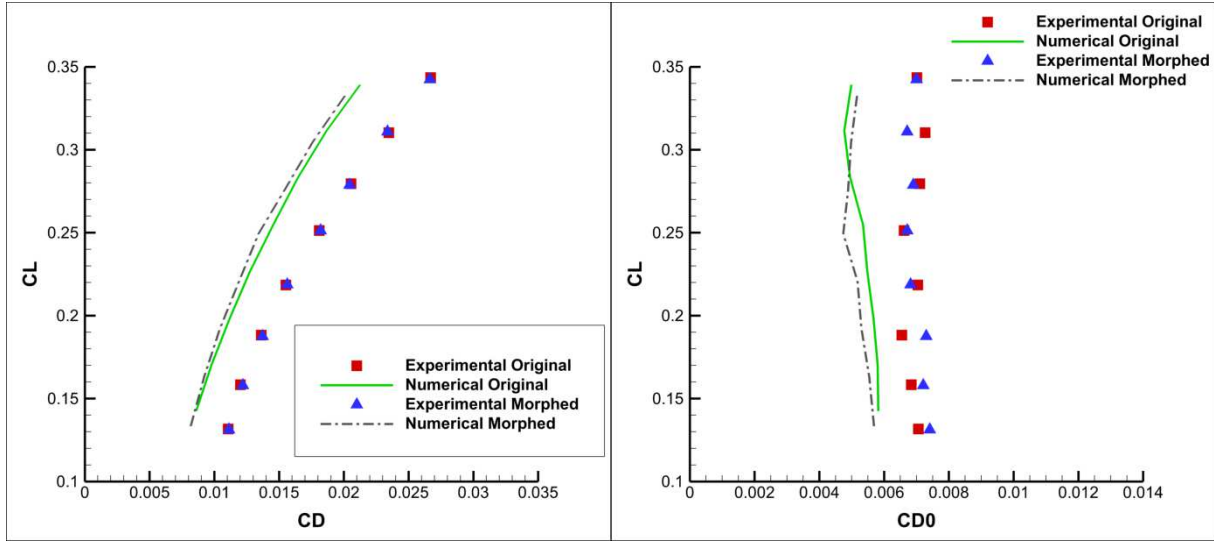


Figure 11 Comparison of the total drag (left) and profile drag at 40% of the span station (right) between original and morphed geometries for the wing with no aileron deflection

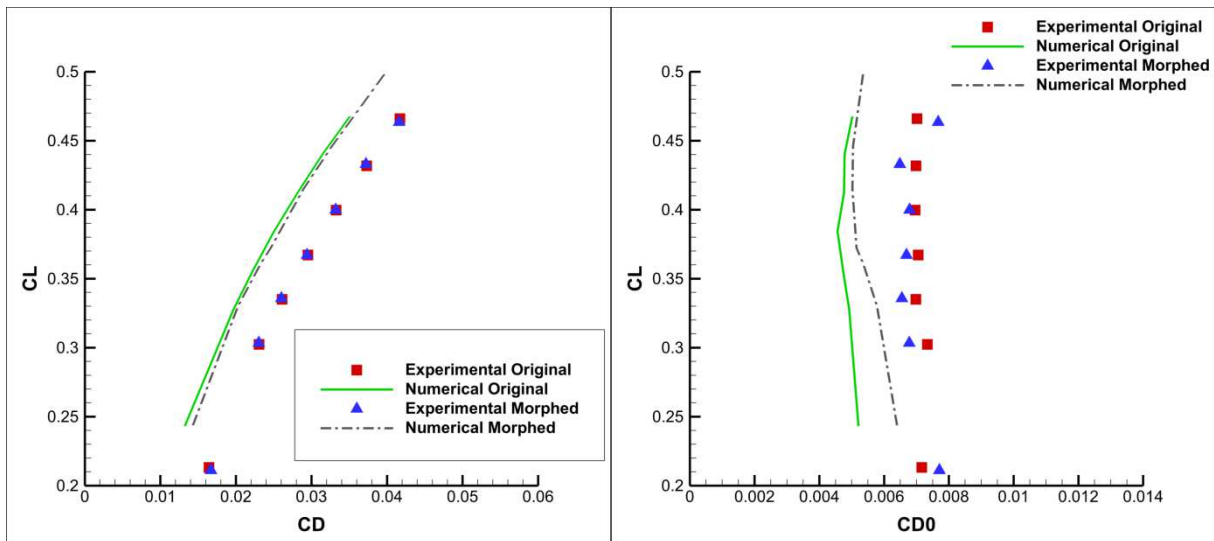


Figure 12 Comparison of the total drag (left) and profile drag at 40% of the span station (right) between original and morphed geometries for the wing with aileron deflected 4 degrees downwards

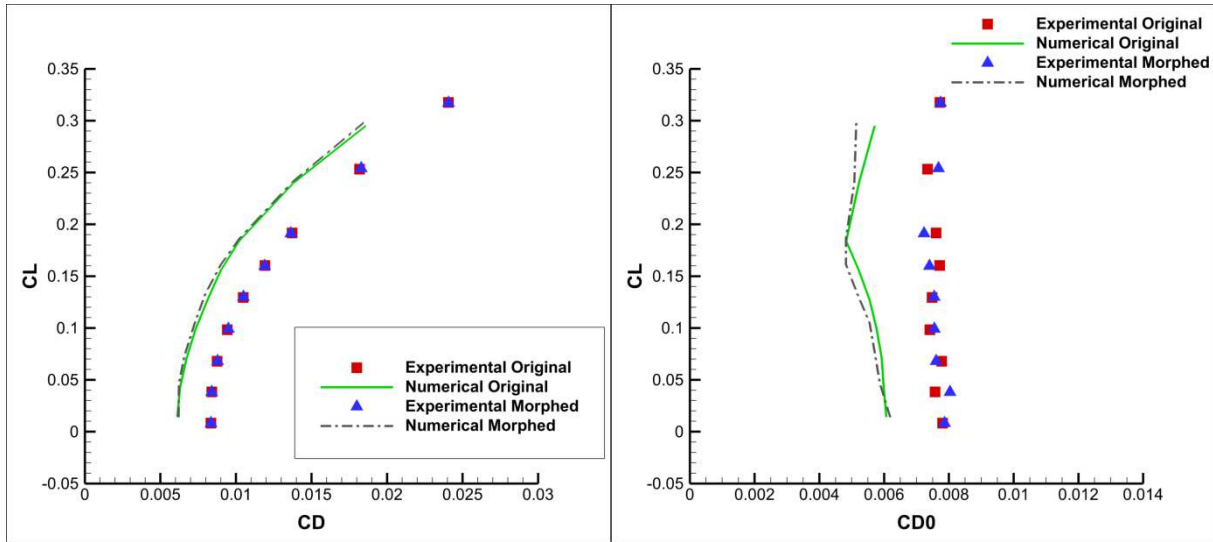


Figure 13 Comparison of the total drag (left) and profile drag at 40% of the span station (right) between original and morphed geometries for the wing with aileron deflected 4 degrees upwards

For the cases without aileron deflection (Figure 11) and the cases with 4 degrees upwards deflection (Figure 13), the two-dimensional optimizations were performed with the objective of delaying the laminar-to-turbulent transition and thus reducing the drag coefficient. This behaviour was also captured by the nonlinear VLM code, for the complete 3D wing model, and small drag reductions can be seen in both the total drag coefficient and the profile drag coefficient at the 40% of the span station. This objective however was only partially obtained experimentally, as in the two Figures there are cases where the drag reduction was obtained, but there are also cases in which a drag increase can be observed. For the cases with 4 degrees downwards aileron deflection (Figure 12), the two-dimensional shape changes were obtained with the objective of advancing the transition point in order to create a more stable turbulent boundary layer, which in turn determines a small drag coefficient increase. Again, the nonlinear VLM code predicted this increase for the wing model, effect which is especially visible in the

section drag coefficient plot. However, the experimentally measured effect of the upper surface morphing was a small reduction of the total drag, with a more significant reduction effect for the 40% of the span section.

The reasons why the behaviour of the experimental results did not match the behaviour of the numerical predictions (2D using XFOIL and 3D using the novel nonlinear VLM) for all the cases are very complex given that the CRIAQ MDO 505 project described in this paper has a multidisciplinary nature. A full analysis of all experimental results must be performed (wind tunnel aerodynamic measurements, actual structural deformation of the upper skin compared to theoretical shapes, control system nonlinearities introduced by the model flexibility) in order to gain a better understanding of the discrepancies.

V. Conclusions

This paper presents a novel nonlinear VLM approach for the calculation of the aerodynamic properties of lifting surfaces. The intensities of the vortex rings were modified by the introduction of a correction term. Viscous aerodynamic forces were calculated by analysing the wing strips with a two-dimensional flow solver and by interpolating the results on the wing surface mesh. The non-linear equations allowing the calculation of the correction terms were constructed by making the pressure coefficient difference equal to the determined viscous pressure coefficient difference, and then the non-linear system was solved using Newton's classic method. Convergence studies were performed on several different test wings and have shown that the nonlinear VLM method required a sufficiently refined mesh in order to achieve mesh-independent results. Validations of the obtained results were performed using wing

performance experimental data available in the literature. Good results were obtained in the estimation of the aerodynamic coefficients for wings with both low and high sweep angles, and both low and high aspect ratios. The nonlinear VLM is applied to the aerodynamic analysis of a morphing wing equipped with a flexible upper surface and controllable rigid aileron. The morphing wing model was designed after the wing tip of a transport aircraft and it was manufactured and fitted with a composite material upper skin. Two-dimensional optimizations were performed in order to determine the skin actuator displacements, as function of the flight condition, with the aim of controlling the extent of the laminar flow region. A comparison was performed for the aerodynamic coefficients of the un-morphed wing, and a good agreement exists between the numerical nonlinear VLM results and the measurements taken during subsonic wind tunnel tests at the CNRC. The drag coefficient comparisons for the morphed wing geometries showed variable levels of agreement, for both total drag and the profile drag at a fixed span-wise station. Due to the complex, multidisciplinary nature of the project, detailed analyses of the experimental results and of the morphing upper skin performance must be performed in order to determine the exact cause of the discrepancies.

Acknowledgments

The authors would like to thank Bombardier Aerospace, Thales Canada, the Consortium for Research and Innovation in Aerospace in Québec (CRIAQ), and the Natural Sciences and Engineering Research Council of Canada (NSERC) for their financial support. Special thanks are due to our collaborators and leaders in this project, namely Mr. Patrick Germain and Mr. Fassi Kafyeke from Bombardier Aerospace, Mr. Eric Laurendeau from Ecole Polytechnique, Mr.

Philippe Molaret from Thales Canada, and Mr. Erik Sherwood and his team from DFS-NRC for the wing model design and fabrication.

References

- [1] [P. Gamboa, P. Alexio, J. Vale, F. Lau, A. Suleman, "Design and testing of a morphing wing for an experimental UAV", RTO-MP-AVT-146, Neuilly-sur-Seine, France, 2007.](#)
- [2] [J. do Vale, A. Leite, F. Lau, A. Suleman, "Aero-structural optimization and performance evaluation of a morphing wing with variable span and camber", Journal of Intelligent Material Systems and Structures, vol. 22 no. 10, pp. 1057-1073, 2011.](#)
- [3] [L. Falcao, A.A. Gomes, A. Suleman, "Aero-structural design optimization of a morphing wingtip", Journal of Intelligent Material Systems and Structures, vol. 22 no. 10, pp. 1113-1124, 2011.](#)
- [4] [G. Diodati, A. Concilio, S. Ricci, A. De Gaspari, C. Liauzun, J.L. Godard, "Estimated performance of an adaptive trailing-edge device aimed at reducing fuel consumption on a medium-size aircraft", 8690-14, Smart Structures/NDE Conference, 10-14 March 2013, San Diego, CA, USA.](#)
- [5] [R. Pecora, F. Amoroso, G. Amendola, A. Concilio, "Validation of a smart structural concept for wing-flap camber morphing", Smart Structures and Systems, vol. 14\(4\), 2014, pp. 659-678.](#)
- [6] [R. Pecora, F. Amoroso, L. Lecce, "Effectiveness of Wing Twist Morphing in Roll Control", Journal of Aircraft, vol. 49, issue 6, 2012, pp. 1666-1674.](#)

- [7] [S. Barbarino, O. Bilgen, R. M. Ajaj, M. I. Friswell, D. J. Inman, “A review of Morphing Aircraft”, Journal of Intelligent Material Systems and Structures, vol. 22\(9\), pp. 823-877, 2011.](#)
- [8] [R.M. Botez, P. Molaret, E. Laurendeau, “Laminar flow control on a research wing: project presentation covering a three-year period”, Canadian Aeronautics and Space Institute Annual General Meeting, January 2007.](#)
- [9] [V. Brailovski, P. Terriault, D. Coutu, T. Georges, E. Morellon, C. Fischer and S. Berube, “Morphing laminar wing with flexible extrados powered by shape memory alloy actuators”, in Proceedings of SMASIS08 ASME Conference on Smart Materials, Adaptive Structures and Intelligent Systems, Ellicott City, Maryland, USA, 2008.](#)
- [10] [L. Pages, O. Trifu, I. Paraschivoiu, “Optimized laminar flow control on an airfoil using the adaptable wall technique”, in Proceedings of the Canadian Aeronautics and Space Institute Annual General Meeting, Toronto, Canada, 2007.](#)
- [11] [C. Sainmont, I. Paraschivoiu, D. Coutu, V. Brailovski, E. Laurendeau, M. Mamou, Y. Mebarki and M. Khalid, “Boundary layer behaviour on an morphing wing: simulation and wind tunnel tests”, in Canadian Aeronautics and Space Institute AERO09 Conference, Toronto, Canada, 2009.](#)
- [12] [T.L. Grigorie, R.M. Botez, A.V. Popov, “Design and experimental validation of a control system for a morphing wing”, AIAA Atmospheric Flight Mechanics conference, Minneapolis, USA, August 2012.](#)

- [13] [A.V. Popov, L. Grigorie, R.M. Botez, M. Mamou, Y. Mebarki, "Modeling and testing of a morphing wing in an open loop architecture", AIAA Journal of Aircraft, vol. 47\(3\), pp. 917-923, 2010.](#)
- [14] [T.L. Grigorie, A.V. Popov, R.M. Botez, "Adaptive neuro-fuzzy controllers for an open loop morphing wing system", Proceedings of the Institution of Mechanical Engineers, Part G: Journal of Aerospace Engineering, vol. 223\(7\), pp. 965-975, 2009.](#)
- [15] [A.V. Popov, L. Grigorie, R.M. Botez, M. Mamou, Y. Mebarki, "Real time airfoil optimisation of a morphing wing in a wind tunnel", AIAA Journal of Aircraft, vol. 47\(4\), pp. 1346-1354, 2010.](#)
- [16] [A.V. Popov, L. Grigorie, R.M. Botez, M. Mamou, Y. Mebarki, "Closed loop control of a morphing wing in a wind tunnel", AIAA Journal of Aircraft, vol. 47\(4\), pp. 1309-1317, 2010.](#)
- [17] [O. Sugar Gabor, A. Koreanschi, "Low - speed aerodynamic characteristics improvement of ATR 42 airfoil using a morphing wing approach", IECON 2012, 38th annual conference of IEEE Industrial Electronics, Aircraft Systems Modeling Section, Montreal, Canada, 25-28 October, 2012.](#)
- [18] [O. Sugar Gabor, A. Simon, A. Koreanschi, R. M. Botez, "Numerical optimization of the S4 Éhecatl UAS airfoil using a morphing wing approach", American Institute of Aeronautics and Astronautics AIAA 32nd Applied Aerodynamics Conference, Atlanta, GA, USA, 16-20 June, 2014.](#)

- [19] [O. Sugar Gabor, A. Koreanschi, R. M. Botez, "An efficient numerical lifting line method for practical wing optimization through morphing", Canadian Aeronautics and Space Institute CASI AERO13 Conference, Toronto, Canada, 30 April-2 May, 2013.](#)
- [20] [O. Sugar Gabor, A. Koreanschi, R. M. Botez, "Optimization of an Unmanned Aerial Systems' Wing Using a Flexible Skin Morphing Wing", SAE International Journal of Aerospace, September 2013, vol. 6\(1\), pp. 115-121, 2013.](#)
- [21] [J. Katz, A. Plotkin, "Low Speed Aerodynamics: From Wing Theory to Panel Methods", McGraw-Hill Inc., New York, 1991.](#)
- [22] [A.B. Neto, R.G.A. Guimaraes, P. Paglione, 2014, "Control-point-placement method for the aerodynamic correction of the vortex and the doublet-lattice methods", Aerospace Science and Technology, vol. 37, p. 117-129.](#)
- [23] [L. Leifsson, K. Slawomir, A. Bekasiewicz, 2014, "Fast Low-fidelity Wing Aerodynamics Model for Surrogate-based Shape Optimization", Procedia Computer Science, vol. 29, p. 811-820.](#)
- [24] [J. Mariens, A. Elham, M.J.L. van Tooren, 2014, "Quasi-Three-Dimensional Aerodynamic Solver for Multidisciplinary Design Optimization of Lifting Surfaces", Journal of Aircraft, vol. 51, no 2, p. 547-558.](#)
- [25] [A. Elham, 2015, "Adjoint quasi-three-dimensional aerodynamic solver for multi-fidelity wing aerodynamic shape optimization", Aerospace Science and Technology, vol. 41, p. 241-249.](#)
- [26] [P. Saffman, "Vortex force and bound vorticity", Vortex Dynamics, Cambridge University Press, Cambridge, 1992.](#)

- [27] [P. Deuffhard, “Newton Methods for Nonlinear Problems: Affine Invariance and Adaptive Algorithms”, Springer Series in Computational Mathematics, Vol. 35. Springer, Berlin, 2004.](#)
- [28] [R. H. Neely, T. V. Bollech, G. C. Westrick, R. R. Graham, “Experimental and Calculated Characteristics of Several NACA 44-Series Wings with Aspect Ratios of 8, 10 and 12 and Taper Ratios of 2.5 and 3.5”, NACA Technical Note no. 1270, Langley Memorial Aeronautical Laboratory, 1947.](#)
- [29] W. C. Schneider, “A Comparison of the Spanwise Loading Calculated by Various Methods with Experimental Loadings Obtained on a 45° Sweptback Wing of Aspect Ratio 8, at a Reynolds Number of 4.0×10^6 ”, NACA Report no. 1208, Langley Memorial Aeronautical Laboratory, 1951.
- [30] J.F. Cahill and S.M. Gottlieb, “Low-Speed Aerodynamic Characteristics of a Series of Swept Wings Having NACA 65A006 Airfoil Sections”, NACA Research Memorandum L50F16, Langley Memorial Aeronautical Laboratory, 1950.
- [31] F. Michaud, “Design and Optimization of a Composite Skin for an Adaptive Wing”, Master of Science Thesis, Ecole de technologie superieure, Montreal, Canada, 2014.
- [32] [M. Drela, “XFOIL: an analysis and design system for low Reynolds number airfoils”, Low Reynolds number aerodynamics, Springer, 1989.](#)
- [33] [A. Koreanschi, O. Sugar Gabor, R. M. Botez, “New Numerical Study of Boundary Layer Behaviour on A Morphing Wing-with-Aileron System”, American Institute of Aeronautics and Astronautics AIAA 32nd Applied Aerodynamics Conference, Atlanta, GA, USA, 16-20 June, 2014.](#)

[34] A. Koreanschi, O. Sugar Gabor, R. M. Botez, “Drag Optimization of a Wing Equipped with a Morphing Upper Surface”, *The Aeronautical Journal*, accepted for publication.